

Research Article

Histology of the optic nerve head with special reference to the layer-specific distribution of composite fibers at and near the lamina cribrosa: An immunohistochemical study using specimens from elderly donated cadavers



Kwang Ho Cho ^{a,*},^{1,2}, Noriyuki Sato ^{b,1}, Masahito Yamamoto ^b, Genji Watanabe ^b, Shuichiro Taniguchi ^b, Gen Murakami ^{b,c}, Shin-ichi Abe ^b

^a Department of Neurology, Wonkwang University School of Medicine and Hospital, Institute of Wonkwang Medical Science, 895, Muwang-ro, Iksan-si, Jeollabuk-do 54538, the Republic of Korea

^b Department of Anatomy, Tokyo Dental College, Tokyo, Japan

^c Division of Internal Medicine, Cupid Clinic, Iwamizawa, Japan

ARTICLE INFO

Article history:

Received 1 December 2022

Received in revised form 5 January 2023

Accepted 7 January 2023

Available online 21 January 2023

Keywords:

Optic nerve head
Lamina cribrosa
Elastic fibers
Glial fibrillary acidic protein
S100 protein
Scleral flange

ABSTRACT

Background: This study aimed to demonstrate the composite fibers of the lamina cribrosa (LC) and their layer-specific distributions. The elastic fiber-rich septa, showing a cribriform arrangement in the optic nerve, may continue into the LC.

Methods: Orbital content, including the long course of the optic nerve, was obtained from 25 elderly cadavers. Sagittal and cross-sections were prepared from each specimen. In addition to elastica Masson staining, immunohistochemistry was performed for elastin, glial fibrillary acidic protein (GFAP), S100 protein (S100), and CD68 in microglia.

Results: The LC beam usually had fewer elastic fibers than the septa, but an elastic fiber-rich zone was observed along the scleral flange. GFAP-positive fibers were rich in the prelaminar area, whereas S100-positive fibers were rich in all layers of the LC. Double-positive (GFAP+/S100+) fibers were present in the prelaminar area. In contrast, S100-single positive fibers were evident in the LC and retrolamellar areas and were likely to insert into a sclera-choroid border area. The density of macrophages and microglia was not different between the septa and LC. Individual variations were observed in the distribution and density of the nerve-associated fibrous tissues.

Conclusion: The LC beam was quite different from the septa in the composite fibers and architecture. Transverse fibers, dominant in the LC beam, corresponded to fibrous processes of astrocytes and other nerve-associated fibrous tissues. Many of these nerve elements suggest low mechanical properties of the LC.

© 2023 Elsevier GmbH. All rights reserved.

1. Introduction

The lamina cribrosa (LC) at the optic nerve head is a collagenous meshwork comprising of abundant combinations of a “pore”

surrounded by a “beam”. The optic nerve fiber bundle passes through each pore (Radius and Gonzales, 1981; Quigley and Addicks, 1981; Elkington et al., 1990). In the inferomedial quadrant or the inner nasal sector, the pores are small, the beam is thin (Radius and Gonzales, 1981; Quigley and Addicks, 1981), and the nerve fiber cytoskeleton is of low density (Kang and Yu, 2015). Ophthalmologists have long compared the LC structure in eyes with or without glaucoma (Downs et al., 2007; Jonas et al., 2012, 2014), measured the stiffness of the LC (Roberts et al., 2010; Midgett et al., 2017; Wang et al., 2017, 2020), and postulated biomechanical models to understand pathological changes by elevated intraocular pressure (Wang et al., 2016, 2017, 2018; Voorhees et al., 2017; Karimi et al., 2021) as

* Corresponding author.

E-mail addresses: neurology@wonkwang.ac.kr, neuro20015@gmail.com (K.H. Cho), spsd66b9@wt.ocn.ne.jp (N. Sato), yamamotomasahito@tdc.ac.jp (M. Yamamoto), watanabegenji@tdc.ac.jp (G. Watanabe), taniguchisuuichirou@tdc.ac.jp (S. Taniguchi), g.murakamisaori@gmail.com (G. Murakami), abesh@tdc.ac.jp (S.-i. Abe).

¹ These authors contributed equally to this work.

² ORCID: 0000-0002-7751-0469.

well as mechanical stresses during eye movement (Wang et al., 2016; Shin et al., 2017).

Recently our group revisited the histological architecture of optic nerve associated fibrous tissues (Cho et al., 2022), i.e., the “dural sheath,” the “sheath of pia mater” (pial sheath), and the “septum or septa” dividing nerve fibers into fascicles. The nerve septa appear in the intracranial course near the chiasma, without continuation to the dura and pia mater. The pial sheath and nerve septa shows strong elastin immunoreactivity. Glial fibrillary acidic protein (GFAP)-positive astrocytes have a linear arrangement along and outside the septa (Cho et al., 2022). The elastin-rich septa continue anteriorly to connect the beams of the cribriform plate (CP) (Triviño et al., 1996). Moreover, the septa extend far anteriorly into the nerve fiber layer of the retina in near-term fetuses (Cho et al., 2022). However, in adults, no research group has examined whether elastic fibers extend from the septa to the CP, possibly because previous studies using immunohistochemistry (IHC) and/or transmission electron microscopy have focused on GFAP-positive fibers in the LC (Elkington et al., 1990; Hernandez, 2000; May, 2008). Optic nerve-associated fibrous tissues contain not only GFAP-positive astrocyte processes but also S100 protein (S100)-positive structures (Cho et al., 2022). S100, a well-known marker of the Schwann sheath, is expressed by some optic nerve astrocytes and the so-called “LC cells” and, unlike astrocytes, the LC cells are positive for smooth muscle actin (Lopez et al., 2020). Astrocyte fine processes line the pores of the LC to provide “glial tubes”. Composite fibers of the LC beam are inserted into the Bruch's membrane and choroid (Jonas et al., 2012; Wang et al., 2021) as well as the scleral flange.

Previous studies have divided the LC into four layers (prelaminar, anterior LC, posterior LC, and retrolaminar layers) (e.g., Kang and Yu, 2015). Beams of the LC insert into the scleral flange and choroid in the posterior and anterior LC, respectively. Knowledge of composite fibers of each layer at and near the LC as well as the optic nerve septa is summarized in Fig. 1. Previous diagrams showed close attachments between adjacent glial tubes around the pores (Radius and Gonzales, 1981; Quigley and Addicks, 1981). However, the present Fig. 1C emphasizes transverse fibers of the beam as the connection between glial tubes because these fibers are shown as “beams” in routine histology in all previous references. Consequently, this study aimed to demonstrate 1) composite fibers of LC beams, including elastic fibers and nerve-associated GFAP-/S100+ fibers (LC cells); 2) their layer-specific distribution at and near the LC; 3) their continuation to the septa of the optic nerve; and 4) the insertion morphology of fibers at the scleral flange. According to Lopez et al. (2020), cultured LC cells are positive for smooth muscle actin antibodies. The fibrous components are likely to be classified into three patterns: double-positive (GFAP+/S100+), single-positive (GFAP+/S100-, GFAP-/S100+), and/or double-negative (GFAP-/S100-). Collagen and elastic fibers should show a third pattern of reactivity. Finally, because the specimens were obtained from elderly cadavers, the morphologies might have been the result of degenerative changes with aging.

2. Material and methods

This study was performed in accordance with the provisions of the Declaration of Helsinki, 1995 (as revised in 2013). To prepare paraffin-embedded histological sections from 25 elderly cadavers, we removed the unilateral orbital contents (15 men, 10 women;

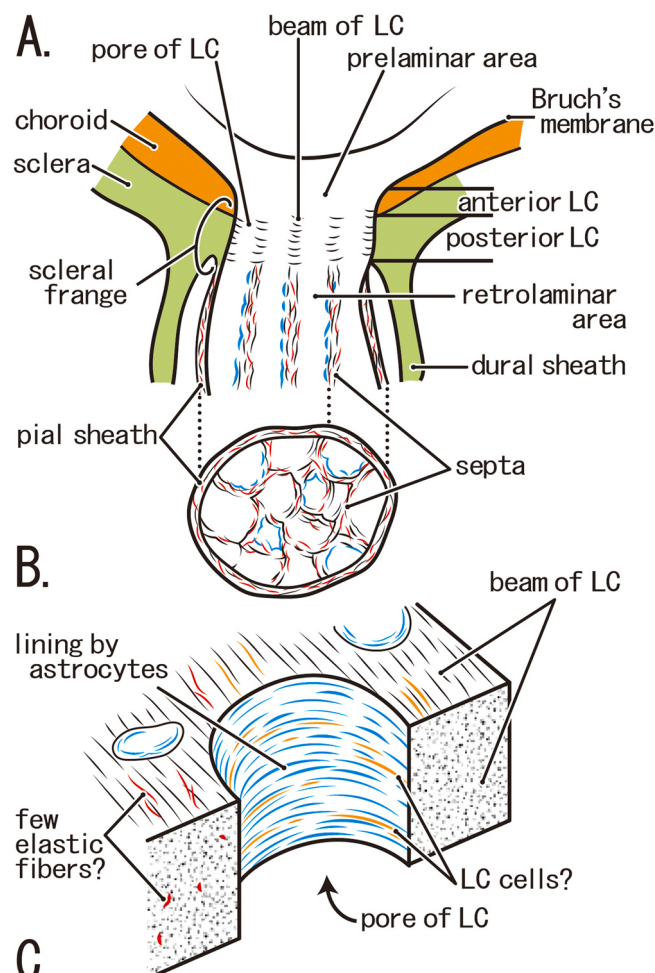
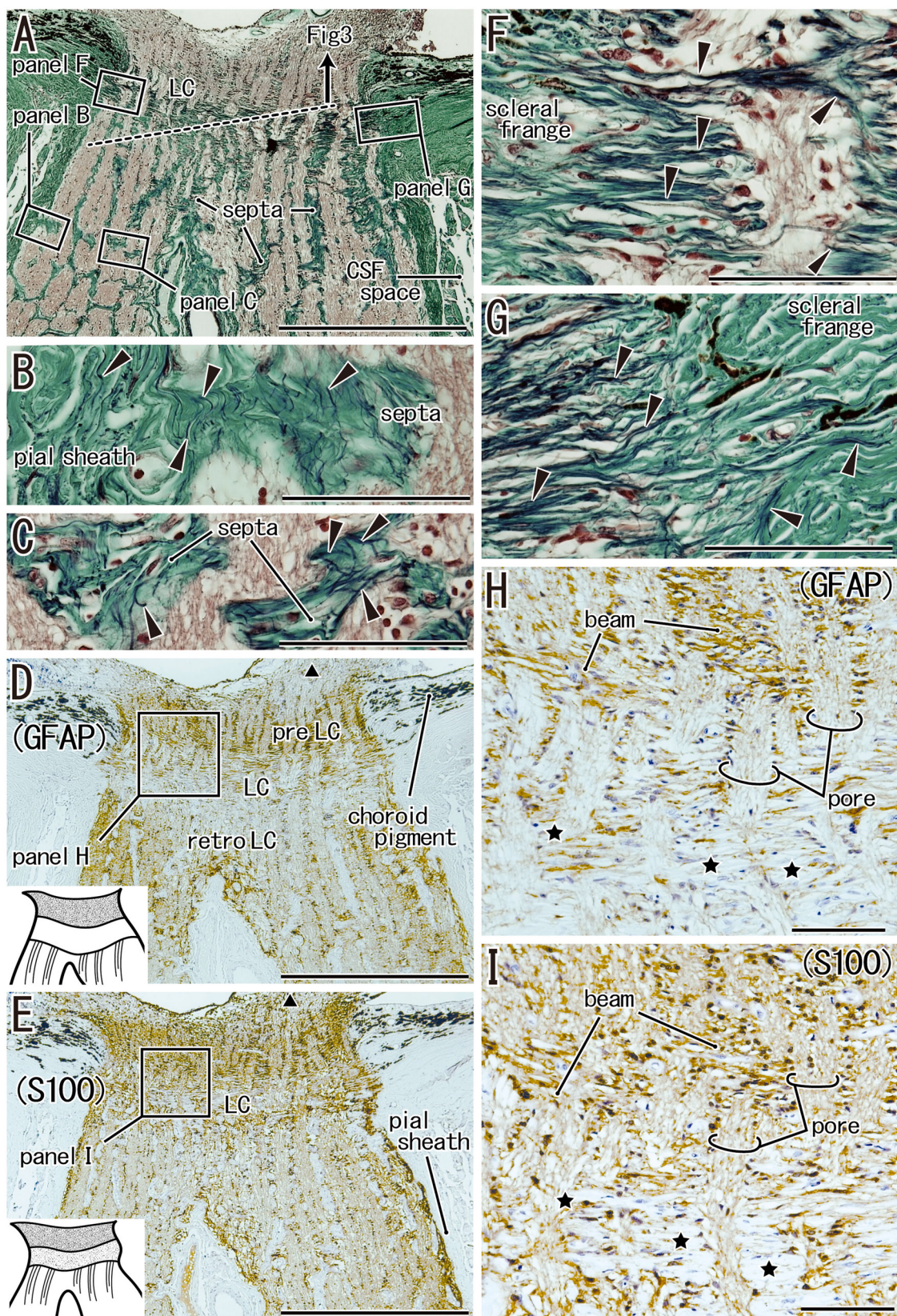


Fig. 1. Schematic representation of fibrous architecture of the lamina cribrosa and the optic nerve. Panel A displays a sagittal view of the lamina cribrosa (LC); the posterior LC is composed of a collagenous beam and a pore for nerve passage. Collagenous fibers were inserted into the scleral flange. In the retrolaminar area, the beam continues to the septa of the optic nerve. The septa and pial sheath contain abundant elastic fibers (red). The septa are lined with astrocytes (blue). Panel B shows a cross-section of the optic nerve at a level distant from the LC. The septa, comprising collagenous (black) and elastic (red) fibers, provide an LC-like architecture although the nerve passage is thicker than the LC. Panel C shows a 3-dimensional model of the beams and pores of the LC according to references. Astrocytes (blue) line the pores to provide a “glial tube” for nerve passage. Panel C contains half of the tube at the center. Glial tubes are mutually connected by the collagenous fibers of the beam. However, the distribution of lamina cribrosa cells (orange) remains unknown (LC cells). Similar to the sclera, the beam may contain a few elastic fibers (red).

71–99 years old; mean age, 85 years at death). All cadavers were donated to Tokyo Dental College for research and education on human anatomy and had been fixed by arterial perfusion of 10 % v/v formalin solution, and stored in 50 % v/v ethanol solution for more than three months. The use of cadavers for research was approved by the ethics committee of the dental college (No. 932). The cause of death was ischemic heart disease or brain disease. We had no information on whether the donors had been suffering from glaucoma.

We divided the orbital content into lateral and medial halves; thus, the optic nerve and LC were also divided sagittally, almost



(caption on next page)

Fig. 2. Sagittal sections of the lamina cribrosa and optic nerve from an 81-years-old woman. Panels A, B, C, F, and G, elastica Masson staining; panels D and H, immunohistochemistry (IHC) of glial fibrillary acidic protein (GFAP); panels E and I, IHC of S100 protein (S100). Panels D and E show the adjacent sections. Panels B, C, F, and G show higher magnification views of squares in panel A. The dotted line in panel A indicates the plane of a cross-section (another half of the same specimen), as shown in Fig. 3. Panels D and E display distributions of astrocytes and the other nerve-associated tissues, respectively, the latter appears denser than astrocytes in the lamina cribrosa (LC). Both GFAP- and S100-positive fibers appear to be inserted into the retina (triangles in panels D and E, respectively). The prelaminar area (preLC) shows strong GFAP reactivity, while the retrolaminar area (retroLC) shows weak reactivity. The positive fiber distribution is summarized in the inserts at the lower angles of panels D and E: S100 reactivity is stronger than that of GFAP in the LC and retroLC. In panels F and G, the beam fiber insertion into the scleral flange contains abundant elastic fibers (arrowheads). Panels H and I exhibit higher-magnification views of the squares in panels D and E, respectively. Stars in panels H and I indicate non-nerve elements (largely collagenous fibers). Panels A, D, and E (or Panels B, C, F, G, H, and I) were prepared at the same magnification (scale bars: 1 mm in panels A, D, and E; 0.1 mm in panels B, C, F, G, and I).

←

along the center. The central artery at the papilla was present in both the lateral and medial halves or in one of the halves. After routine procedures for paraffin-embedded histology, one half was used for serial sagittal sections, including a long posterior course of the optic nerve, while the other half was used for serial cross-sections of the LC (5–7 μm in thickness). A pair of paraffin blocks, which contained a larger area of the LC insertion to the scleral flange, was used for cross sections according to surface observations. The sections were stained with elastica Masson staining and IHC (antibodies, see below). In elastica Masson staining (a variation of Masson-Goldner staining) (Motohashi et al., 1995; Hayashi et al., 2010), elastic fibers were stained black, while muscles were bright red. All histological photographs were taken using a Nikon Eclipse 80 microscope.

The primary antibodies used were: 1) rabbit polyclonal anti-human GFAP (1:100; Dako Cytomation, Kyoto, Japan; catalog number Z0334); 2) mouse monoclonal anti-human S100 protein (1:100; Dako Z0311; Dako, Glostrup, Denmark); 3) mouse monoclonal anti-bovine alpha-elastin (1:20; ab9519; Abcam, Cambridge, UK); 4) mouse monoclonal anti-human alpha-smooth muscle actin or SMA (1:800; Dako M0851; Dako, Glostrup, Denmark) and; 5) mouse monoclonal anti-human CD68 (1:200; Dako N0814; Dako, Glostrup, Denmark). Antigen retrieval with trypsin was performed for the immunohistochemical analysis of elastin, SMA, and CD68. The secondary antibody (incubation for 30 min; dilution, 1:1000; Histofine Simple Stain Max-PO, Nichirei, Tokyo) was labeled with horseradish peroxidase (HRP), and antigen-antibody reactions were detected by HRP-catalyzed reaction with diaminobenzidine (incubation for 3–5 min; Histofine Simple Stain DAB, Nichirei, Tokyo). Hematoxylin counterstaining was performed for the same samples. A negative control without the first antibody was set up for each specimen. The anti-SMA antibody used in the present study has been reported to stain the endothelium of arteries and veins, as well as smooth muscle, but does not react with the lymphatic endothelium (Hayashi et al., 2008).

3. Results

3.1. Overview of present figures

As both sagittal and cross sections were prepared in the unilateral orbital content from each of the 25 cadavers, we were able to show a combination of two planes from each of the cadavers (Figs. 2 and 3 from an 81-years-old woman; the left and right halves of Fig. 4 from an 86-years-old man). These figures contain both photographic demonstrations of elastica Masson staining and IHC. In Figs. 2–4, panel A displays the topographical anatomy in the sagittal plane. We sometimes failed to make a real cross plane at the right angle to the sagittal sections of the same specimen; thus, the sections were likely to be oblique and contained both the LC and retrolaminar areas

(Fig. 3A). A positive area in the IHC of elastin (Figs. 3D and 4B) is not always the same as a dense area of elastic fibers in elastica Masson staining (Figs. 3BC and 4 FG) because IHC demonstrates both elastic and oxytalan fibers. To the best of our knowledge, this is the first report of elastic fibers inserted into the scleral flange. Using sagittal sections from four cadavers, Figs. 5 and 6 show individual differences in the distribution of GFAP-positive astrocytes and S100-positive fibers, including LC cells. This is the first report of the distribution of S100 single-positive fibers (GFAP-/S100+) at and near the LC. The distribution of CD68-positive microglia and macrophages in the LC and septa distant from the LC is shown in Fig. 7. In addition, a limited demonstration of SMA expression is shown in Fig. 3D because there is no reaction with the LC components except for the vascular endothelium.

3.2. Elastic fibers

Elastic fibers tended to run along collagenous fiber bundles (green-colored fibers in elastica Masson staining) at the insertion to the scleral flange, while they ran irregularly in the septum, dural sheath, and scleral flange. The pial sheath contained longitudinal elastic fibers (Fig. 2B); thus, they appeared wavy because they were thick but fragmented in cross-sections (Fig. 3B). In elastin IHC, rather than LC, the septa and pial sheath showed high reactivity (Fig. 3D). Elastin is also abundant along the central artery of the retina. In contrast to elastin IHC, elastica Masson staining clearly demonstrated fine elastic fibers at higher magnification (20X or 40X at objective; Figs. 2BC, 3BC, and 4G). The LC beam usually contains fewer elastic fibers than the septa of the optic nerve. However, in five cadavers we found that elastic fibers of the LC beam intermingled with those in the scleral flange (Fig. 2 FG). The insertion fibers were thicker than those in the scleral flanges (Fig. 3C). Moreover, in the LC of the other 2 cadavers, an “elastin-rich zone” was evident along the scleral flange (Fig. 4F-H). This circular zone appeared to be separated and 0.2–0.3 mm distant from the flange in the cross sections (Fig. 4F). In the rich zone, the LC beam and flange expressed strong elastin reactivity, but elastic fibers were not clearly identified in elastica Masson staining (Fig. 4GH). Overall, there was an individual difference in the distribution and density of the elastic components at and near the LC. Collagenous fiber bundles tended to be rich and thick in zones or areas rich in elastic fibers. Cross-sections showed that thicker LC beams contained greater numbers of collagenous fiber bundles.

3.3. Nerve-associated fibrous tissues

The nerve-associated fibrous tissues included GFAP-positive astrocytes, S100-positive LC cells, and other unclassified fibrous cells. Astrocytes usually showed a positive reactivity for S100 (GFAP

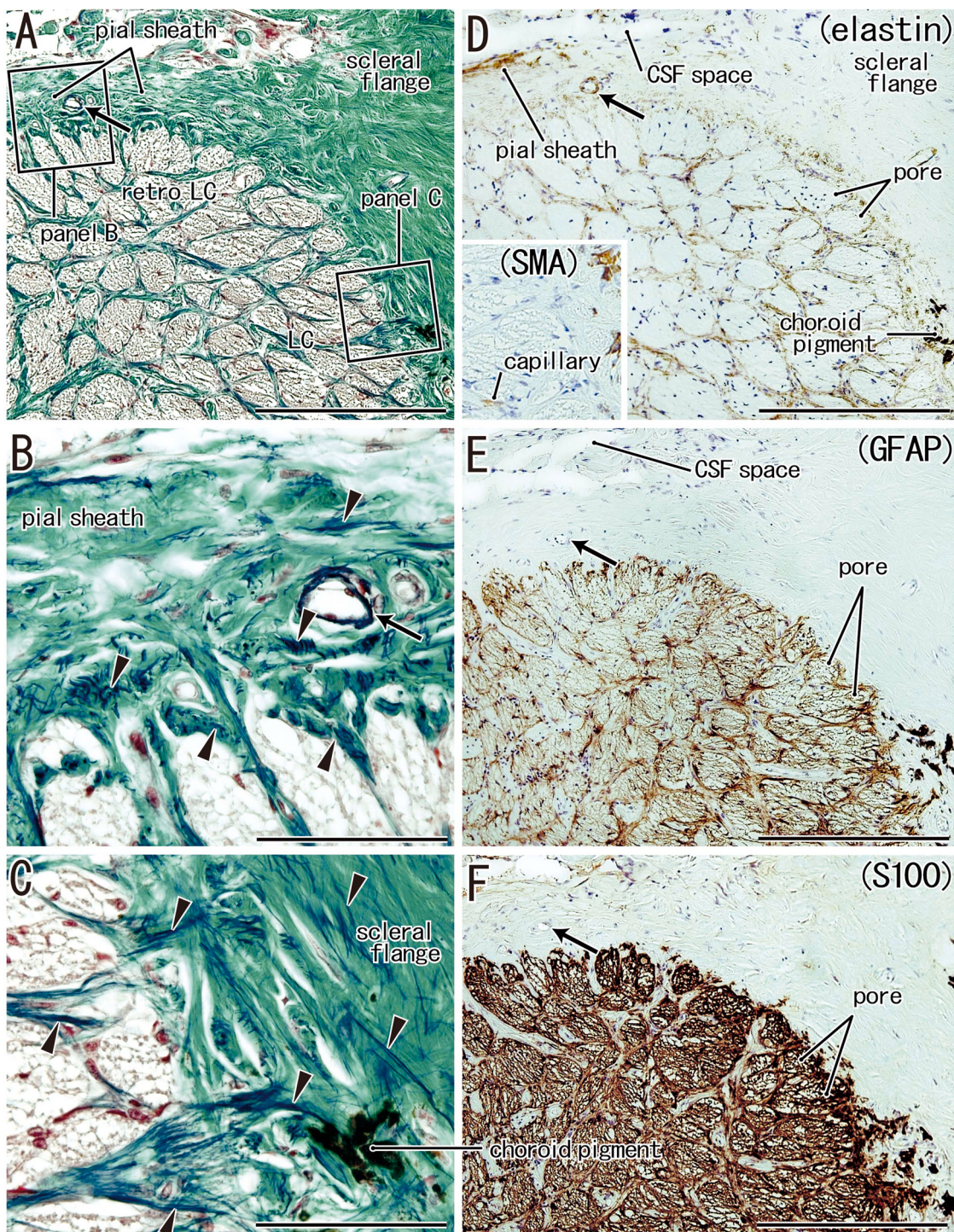
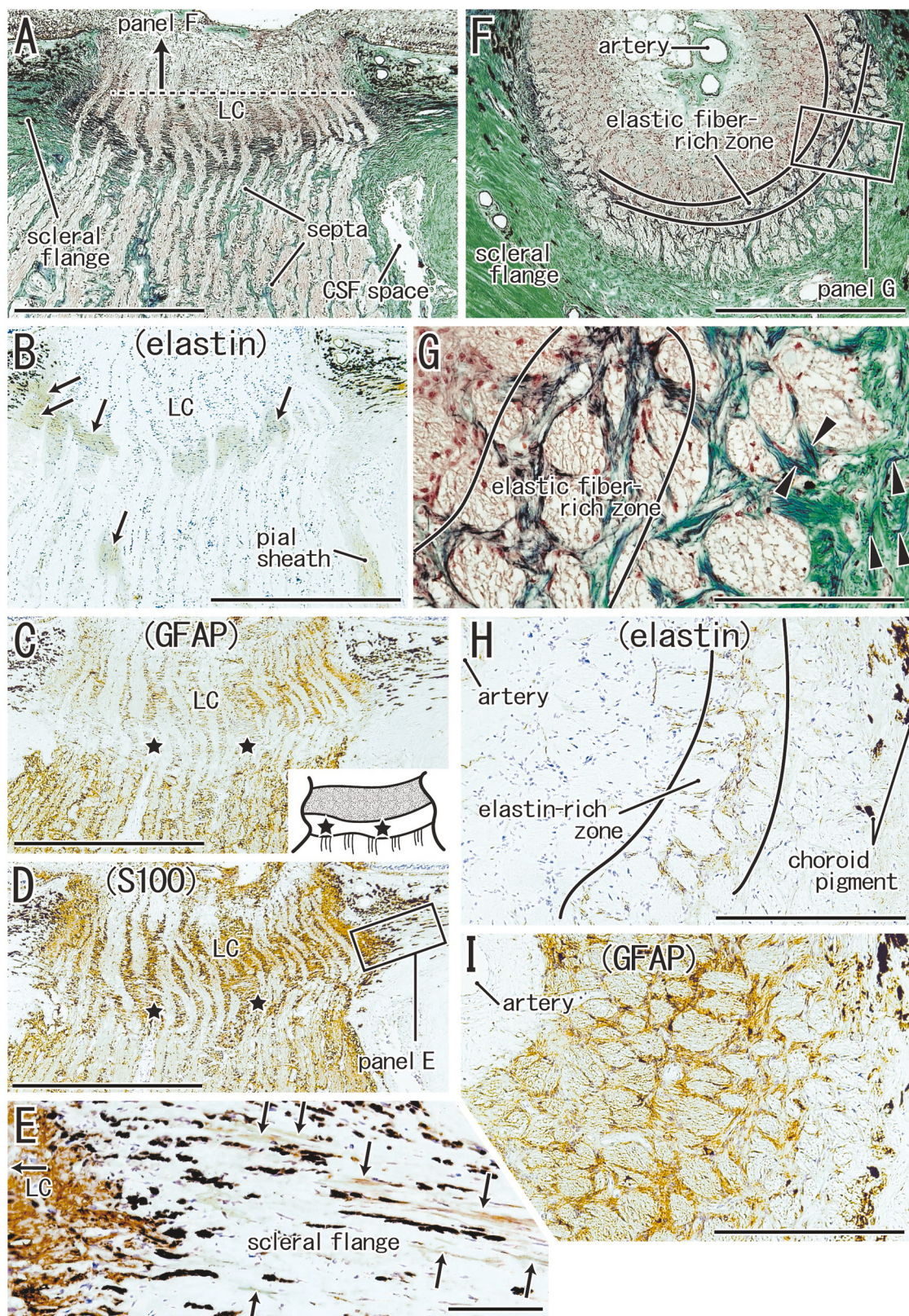


Fig. 3. Cross sections of the lamina cribrosa and retrolaminar area from an 81-years-old woman. The same specimen as shown in Fig. 2. Panels A-C, elastica Masson staining; panel D, immunohistochemistry (IHC) of elastin; panel E, IHC of glial fibrillary acidic protein (GFAP); panels F, IHC of S100 protein (S100). An insert at the lower angle of panel D, showing an LC area corresponding to the lower right quarter of panels D-F, contains a capillary positive for IHC of smooth muscle actin (SMA). Panels D-F show adjacent sections. Panels B and C show higher magnification views of the squares in panel A. For correspondence between panels, an arrow in panels A, B, D, E, and F indicates the same artery. Because the sectional plane is tilted incidentally, both the lamina cribrosa (LC) and retrolaminar area (retroLC) can be seen in a single section (panel A). Elastic fibers (arrowheads) of the septa are wavy and inserted into the pial sheath (panel B), while those of the lamina cribrosa beam are straight and inserted into the scleral flange (panel C). In panel D, the pial sheath is highly reactive in the IHC of elastin. S100-positive fibers (panel F) reinforce GFAP-positive glial tubes around the pores (panel E) and connect between them. Panels A, D, E, and F (or Panels B and C) were prepared at the same magnification (scale bars: 1 mm in panels A, D, E, and F; 0.1 mm in panels B and C).



(caption on next page)

Fig. 4. A combination of sagittal and cross sections of the lamina cribrosa and optic nerve from an 86-years-old man. Panels A-E, sagittal sections; panels F-I, cross sections of another half of the same specimen. Panels A, F, and G, elastica Masson staining; panels B and H, immunohistochemistry (IHC) of elastin; panels C and I, IHC of glial fibrillary acidic protein (GFAP); panels D and E, IHC of S100 protein (S100). Panels A-D and panels F, H, and I show the adjacent sections. Panels E and G exhibit higher-magnification views of the squares in panels D and F, respectively. The dotted line in panel A indicates the sectional plane of panel F. In panels A-D, a caption "LC" (lamina cribrosa) is placed on the same site to correspond between the panels. In panel B, elastin reactivity is observed in the pial sheath, septa, and lamina cribrosa beam (arrows). Panels C and D display distributions of GFAP-positive and S100-positive fibers, respectively; the former is almost absent in the retrolaminar area (stars; shown also in an insert at the right lower angle of panel C), while the latter is dense. In panel E, S100-positive fibers of the LC insert deeply into the scleral flange near the choroid, and therein, other weakly positive fibers are seen passing between choroid pigments (arrows). In panels F-H, elastin-rich and elastic fiber-rich zones are observed along the scleral flange. Fragmented elastic fibers are also observed in the LC insertion into the flange (arrowheads in panel G). The elastic beams also contain GFAP-positive fibers (panel I). Scale bars: 1 mm in panels A-D and F, H, and I; 0.1 mm in panels E and G.

+/S100 +). The third category included S100-positive cells other than astrocytes or LC cells; the latter existed in the optic nerve distant from the LC (Fig. 2E). Indeed, most GFAP-positive fibers were likely to correspond to the slender processes of astrocytes, but they contained fibers positive or negative for S100 reactivity (GFAP+/S100 +; GFAP-/S100 -). As we recently showed (Cho et al., 2022), the septa, which are abundant collagenous and elastic fibers, were lined by GFAP-positive cell bodies (astrocytes) and S100-positive fibers. Similarly, the pial sheath was lined with a thick lamina comprising S100-positive fibers (Fig. 2E). Therefore, rather than a dichotomy such as astrocytes or LC cells, we describe site-by-site immunoreactivity at and near the LC.

Longitudinal nerve-associated fibers were evident in the prelaminar area, most of which were double-positive (GFAP+/S100 +). In contrast, nerve-associated transverse fibers were evident in the LC and retrolaminar areas. Possibly because of the double positivity of GFAP and S100, S100-positive fibers were usually observed in all layers (Figs. 2E, 4D, and 5H). However, sometimes they were poor in the LC (Fig. 5BF) or relatively few in number in the retrolaminar area (Fig. 5D). The distribution of nerve-associated fibers is summarized in a small insert at the lower angle of each panel of sagittal sections. The S100-single positive transverse fibers in the LC (possibly LC cells) provided 2–4 layers in the posterior LC and retrolaminar area; in the layers, they occupied almost all parts of the LC beam (Fig. 6). They were likely to be inserted into the scleral flange and sclera-choroid border area (Fig. 4DE). Fig. 6 also shows that the glial tube of pores was lined by both double-positive fibers (GFAP+/S100+) and S100 single-positive fibers (Fig. 6AB), that is, astrocytes, LC cells, and others.

3.4. Other observations

Black pigment cells of the choroid usually extend to the scleral flange near the LC. Collagenous fiber bundles in the LC were identified as non-reactive structures by immunostaining for GFAP or S100 (stars in Fig. 2HI). Along the central artery of the retina, no reactive area was evident (Fig. 2E and 5BH). The number of CD68-positive macrophages and microglia was different between specimens, but the density was not different between the septa and LC (Fig. 7). The positive cells tended to arrange along the transverse fibers connecting the LC beams. In the optic nerve distant from and posterior to the LC, the positive cells appeared outside the septum. Finally, in spite of individual differences in the density of elastic and nerve-associated fibers, there was a basic rule in the composite fibers of each layer at and near the LC (Fig. 8 and its associated table). The composite fibers and their arrangement in the septa were changed in the retrolaminar area to provide an LC-specific configuration. Likewise, at the LC-prelaminar border, the transverse fibers were suddenly lost.

4. Discussion

4.1. Nerve-associated fibrous tissues

GFAP+/S100- fibers are processes of astrocytes, while astrocytes are also likely to be GFAP-/S100+ according to the observations of the septa of the optic nerve (Cho et al., 2022). Astrocytes bundle retinal ganglion axons to make "glial tubes" in the LC (Fig. 1). On the posterior side of the LC, this basic configuration is maintained because the septa of the optic nerve contain abundant double-positive cells at aspects facing the retinal axon bundles (Cho et al., 2022; Fig. 8). The most striking feature of the present results was the fact that without the coexistence of astrocytes, GFAP-/S100+ fibers were likely to occupy a large area in the LC and retrolaminar area. The amount often or sometimes appeared to be greater than that of the collagenous and elastic fibers. Classical diagrams (e.g., Triviño et al., 1996) provided an image that, in the LC, glial tubes of astrocytes are mutually connected by transverse fibers that correspond to the process of astrocytes. However, Fig. 6 shows all transverse fibers likely comprising S100 single-positive.

Notably, in contrast to peripheral nerves (e.g., the oculomotor nerve shown in Cho et al., 2022), the present S100 single-positive fibers did not run longitudinally, but transversely in the LC and retrolaminar area. We considered the S100 single-positive fibers as not only LC cells, but also other types of nerve-associated fibrous tissues. These nerve-associated tissues in the LC areas should have physiological importance for maintaining retinal ganglion axons. The LC beam contained no or few capillaries, in contrast to the septa, which always contained vessels. According to Lopez et al. (2020), glial tubes contain both astrocytes and LC cells (GFAP-/S100+/SMA+). In contrast to the cultured LC cells established by Lopez et al., no SMA reactivity was observed in the present section of the LC; this difference might also suggest great heterogeneity of nerve-associated cells in the LC. Finally, we did not reject the hypothesis that in the LC of aged persons, the nerve-associated fibrous tissue replaces the collagenous and/or elastic fibers of the LC. Because the S100 protein causes glial proliferation (Zimmer et al., 1995), its high content in the LC might correspond to an overexpression against cell death of astrocytes with age. Finally, the S100-positive and/or GFAP-positive longitudinal fibers appeared to be dominant in the prelaminar area. Since the area contained no or few collagen and elastic fibers, these nerve-associated fibers seemed to mechanically support ganglionic axons converging to the optic nerve head.

4.2. Collagenous and elastic fibers

Although the LC beam appears to continue to the septa of the optic nerve in routine histology, it was quite different in terms of composite fibers and architecture (Fig. 8). As Thale et al. (1996)

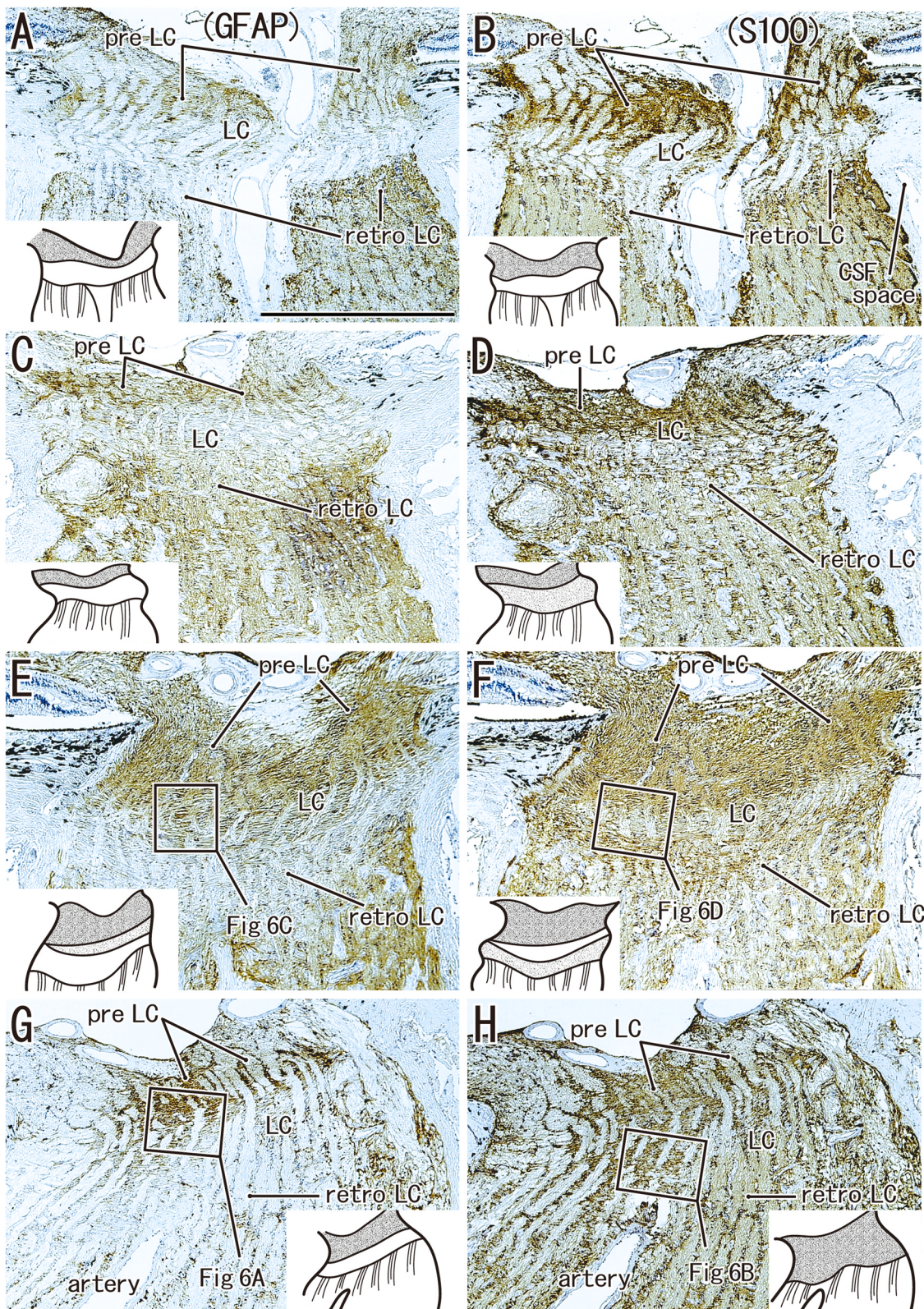


Fig. 5. Individual variation in fiber distribution of the lamina cribrosa beam; sagittal section immunohistochemistry using specimens from four elderly cadavers. Panels A and B, a 75 years-old man; panels C and D, 76-years-old man; panels E and F, a 92 years-old woman, panels G and H, an 85 years-old woman. Panels A, C, E, and G, immunohistochemistry (IHC) of glial fibrillary acidic protein (GFAP); panels B, D, F, and H, IHC of S100 protein (S100). The positive fiber distribution is summarized in inserts at the lower angles of all panels; both GFAP-positive and S100-positive fibers are dense in the preliminar area (preLC) of the four specimens. In the LC, GFAP reactivity is relatively strong (panel E) or weak (panels A, C, and G). Likewise, S100-reactivity is relatively strong (panels D and H) or weak (panels B and F) in the LC. Panels E and G show GFAP-negative retrolaminar area (retroLC). Overall, in the LC and/or retroLC, the density of astrocytes and lamina cribrosa cells is likely to show an individual variation. The squares in panels E–H are shown in Fig. 6 at higher magnification for further discrimination of lamina cribrosa cells from astrocytes. All panels were prepared at the same magnification (scale bar in panel A: 1 mm).

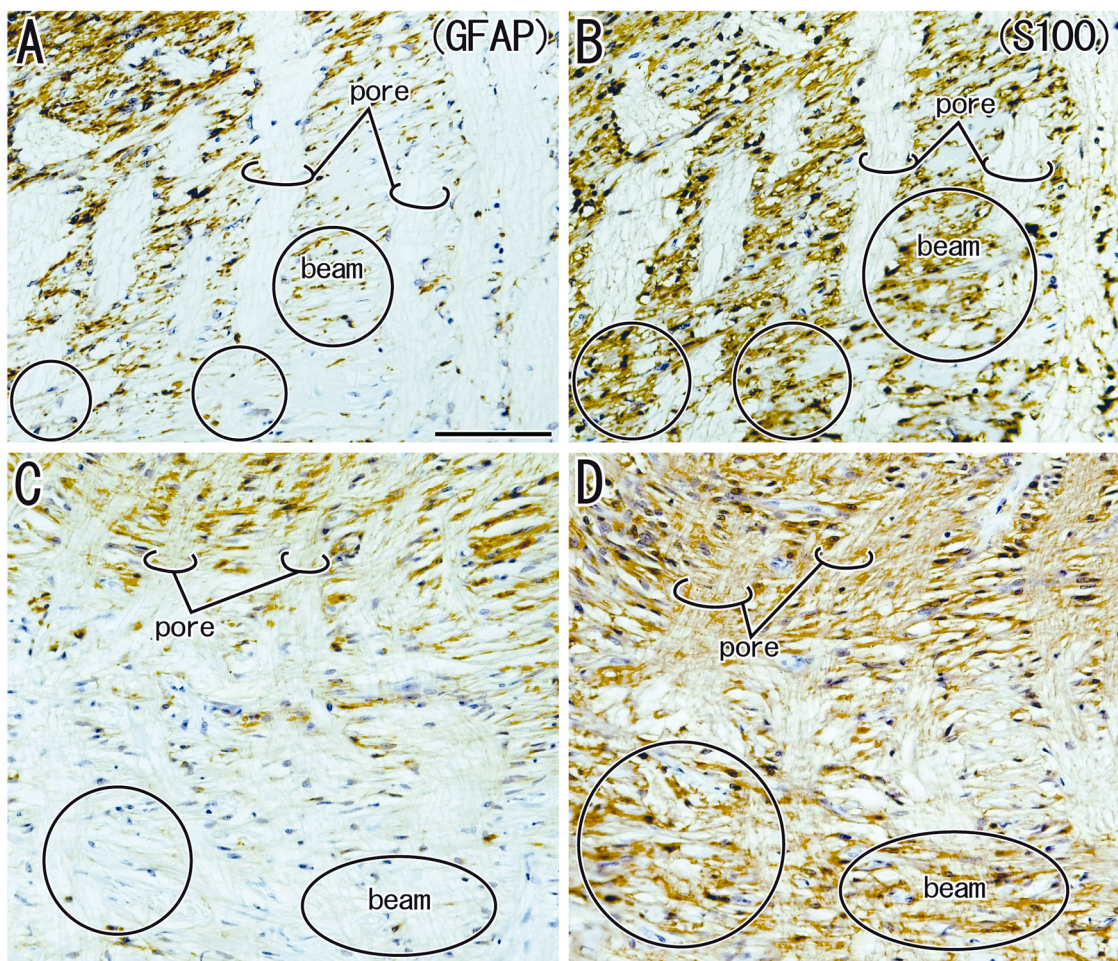


Fig. 6. S100+/GFAP- lamina cribrosa cells and the other fibrous components; sagittal section immunohistochemistry using specimens from two elderly cadavers. Panels A and B (adjacent sections), an 85 years-old woman; panels C and D (near sections), a 92 years-old woman. Panels A and C, immunohistochemistry (IHC) of glial fibrillary acidic protein (GFAP); panels B and D, IHC of S100 protein (S100). Abundant S100-positive fibers (circles in panels B and D) appear to be negative in the IHC of GFAP (circles in panels A and C). Lower magnification views are shown in Fig. 5E-H. All panels were prepared at the same magnification (scale bar in panel A: 0.1 mm).

demonstrated using scanning electron microscopy, transverse collagenous fibers were dominant in the LC beam in contrast to the dominance of irregularly arrayed fibers in the septa; the fiber direction drastically changed in the retrolaminar area. Thus, the retrolaminar area might be weaker than the LC itself against the tensile stress. Elastic fibers in the LC beam were much lower in density than the septa; elastic fibers in the LC beam seemed to be concentrated in a circular zone near and along the scleral flange, not at the insertion itself. Thus, in contrast to collagenous fibers, elastic fibers were not a major factor against the mechanical stress from the LC to the sclera, and vice versa. Collagenous fiber bundles tended to be rich and thick in zones or areas rich in elastic fibers. Cross-sections showed that thicker LC beams contained greater numbers of collagenous fiber bundles. The sclera is known to contain elastic fibers (Marshall, 1995; Quigley et al., 1991; Gelman et al., 2010) although elasticity largely depends on interwoven collagenous fibers (Wang et al., 2020). The density of elastic fibers was higher in the scleral flange than in the other parts of the sclera. At the insertion, the elastic

fibers in the LC beam and scleral flange intermingled. However, in mice, regularly arrayed thin elastic fibers of the LC attach to the scleral flange, but they do not intermingle with elastic fibers in the sclera (Gelman et al. (2010)), which might make the mouse LC weaker than humans.

We noted a circular “elastin-rich zone” of the LC along and 0.2–0.3 mm distant from the scleral flange because of the discrepancy between the strong elastin reactivity in IHC and the unclear demonstration of fibers in elastica Masson staining. However, without observations using transmission electron microscope, we were unable to identify whether oxytalan or unmatured fibers occupied the circular zone.

4.2.1. Concluding remarks

Fig. 8 shows the basic pattern of the LC composite fibers. We also demonstrated individual differences in the density and distribution of the nerve-associated tissues. However, the lower density of GFAP-positive fibers in the LC might not simply be related to the decreased

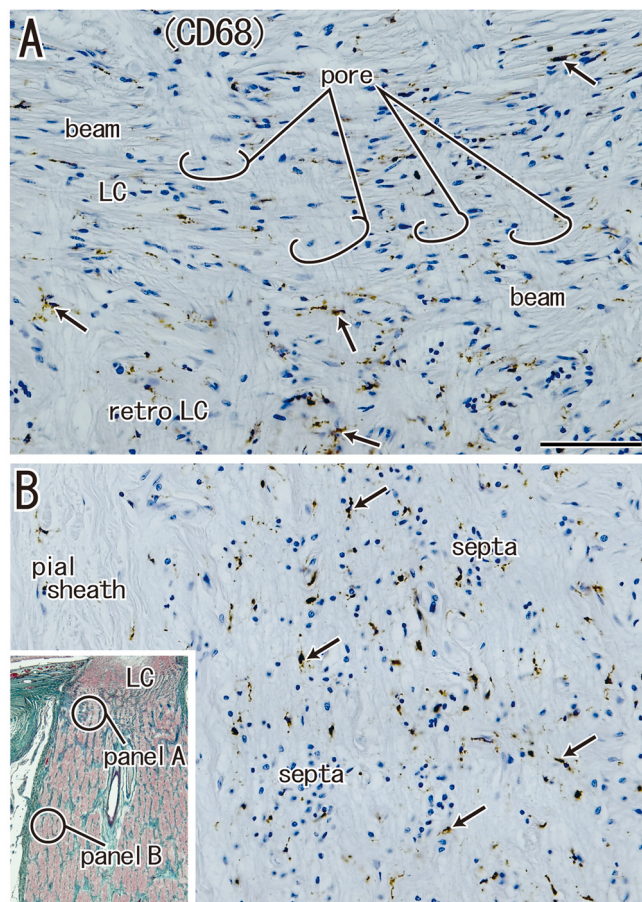


Fig. 7. CD68-positive microglia and macrophage in the optic nerve. Sagittal sections from a 92-years-old woman (the same specimen is shown in Figure 5EF). Panel A displays CD68-positive cells (arrows) in the lamina cribrosa (LC) and retrolaminar area (retroLC), while panel B displays positive cells in the septa. The sites of these panels are shown in an insert at the lower angle of panel B. Panels A and B were prepared at the same magnification (scale bar in panel A: 0.1 mm).

trophic function of retinal axons. The Schwann sheath (GFAP-/S100+) also plays a trophic role, although no chemical barrier has been hypothesized. However, little or no information is available about the physiological roles of nerve-associated tissues other than astrocytes. From a mechanical viewpoint, LC may be recognized as a modified continuation or an analogy of the sclera. However, many nerve-associated tissues in the LC beam suggest poor mechanical properties, especially in aged persons. No distinct difference in the density of macrophages or microglial cells suggested little or no difference in the number of dying cells between the LC and the septa. Therefore, the mechanical load may not be significantly different between the two supportive structures. Further immunohistochemical studies using specimens obtained from young individuals are necessary. Because the present result of S100 protein distribution was almost consistent with that of mass spectrometry (Anderson et al., 2015), imaging technology using healthy volunteers may be better than the histology of cadavers for understanding individual differences, including changes with age.

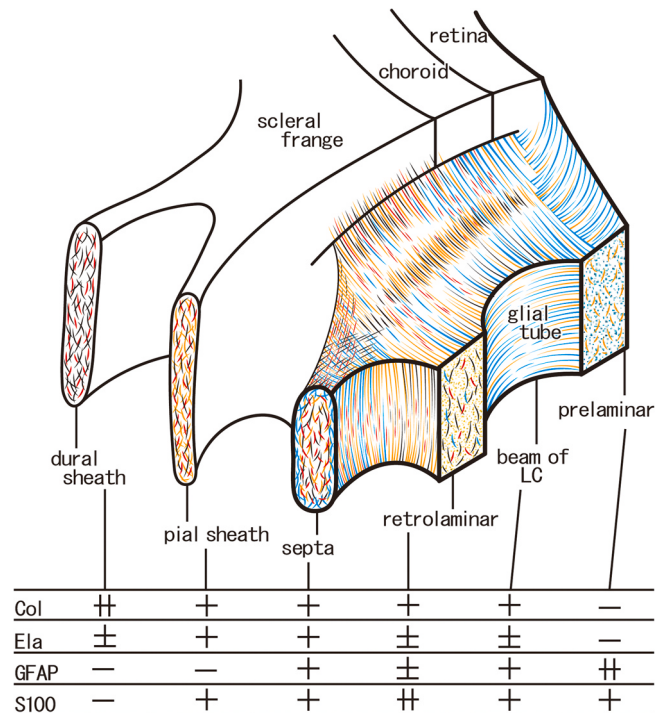


Fig. 8. Schematic representations of fibrous architecture at and near the lamina cribrosa according to the present observations. The composite fibers and their arrangement in the septa were changed in the retrolaminar area to provide an LC-specific configuration. Likewise, at the LC-prelaminar border, the transverse fibers were suddenly lost. Colors of lines: black, collagenous fibers; red, elastic fibers; blue, astrocytes; orange, nerve-associated fibrous tissues other than astrocytes (e.g., lamina cribrosa cells). A table below the scheme summarizes the density of fibrous contents in each of the areas: Col, collagen type 1 fibers; Ela, elastic fibers; GFAP, glial fibrillary acidic protein-positive fiber-like processes of astrocytes; S100, S100-protein positive fibers that are likely to include both astrocytes and lamina cribrosa cells.

5. Study limitations

The density of the fibrous component was not analyzed because of the difficulty in counting the numbers in the section. In IHC, an individual difference in distribution was difficult to discriminate from another difference in reactivity owing to the lag time until postmortem treatment.

Funding

This study was supported by the Wonkwang University in 2023.

CRediT authorship contribution statement

Kwang Ho Cho: Conceptualization (equal); Funding acquisition (lead); Writing – original draft (equal); Writing – review & editing (equal). **Noriyuki Sato:** Conceptualization (equal); Writing – original draft (equal); Methodology (equal). **Masahito Yamamoto:** Conceptualization (equal), Methodology (lead), Formal analysis (equal). **Genji Watanabe:** Methodology (equal), Data curation (equal). **Shuichiro Taniguchi:** Methodology (equal); Data curation (equal).

(equal). **Gen Murakami:** Conceptualization (equal); Writing – review & editing (equal); Supervision (lead). **Shin-ichi Abe:** Conceptualization (equal); supervision (supporting); Writing – review & editing (equal). All authors have read and approved the manuscript.

Ethical statement

The use of cadavers for research was approved by the ethics committee of the Tokyo Dental College (No. 932).

Declaration of Competing interest

The authors declare that they have no known competing financial interests or personal relationships that could have appeared to influence the work reported in this paper.

References

- Anderson, D.G., Spraggins, J.M., Rose, K.L., Schey, K.L., 2015. High spatial resolution imaging mass spectrometry of human optic nerve lipids and proteins. *J. Am. Soc. Mass Spectrom.* 26, 940–947.
- Cho, K.H., Takahashi, A., Yamamoto, Y., Hirouchi, H., Taniguchi, S., Murakami, G., Abe, S., 2022. Optic nerve-associated connective tissue structures revisited: a histological study using human fetuses and adult cadavers. *Anat. Rec.* 305, 3516–3531. <https://doi.org/10.1002/ar.24925>
- Downs, J.C., Yang, H., Girkin, L., Sakata, A., Bellezza, H., Thomson, H., Burgoyne, C.F., 2007. Three-dimensional histomorphometry of the normal and early glaucomatous monkey optic nerve head: neural canal and subarachnoid space architecture. *IOVS* 48, 3195–3208.
- Elkington, A.R., Inman, C.B.E., Steart, P.V., Weller, R.O., 1990. The structure of the lamina cribrosa of the human eye: an immunohistochemical and electron microscopical study. *Eye* 4, 42–57.
- Gelman, S., Cone, F.E., Pease, M.E., Nguyen, T.D., Myers, K., Quigley, H.A., 2010. The presence and distribution of elastin in the posterior and retrobulbar regions of the mouse eye. *Exp. Eye Res.* 90, 210–215.
- Hayashi, S., Murakami, G., Ohtsuka, A., Itoh, M., Nakano, T., Fukuzawa, Y., 2008. Connective tissue configuration in the human liver hilar region with special reference to the liver capsule and vascular sheath. *J. Hep. Bil. Pancr. Surg.* 15, 640–647.
- Hayashi, T., Kumasaka, T., Mitani, K., Yao, T., Suda, K., Seyama, K., 2010. Loss of heterozygosity tuberous sclerosis complex genes in multifocal micronodular pneumocytoma hyperplasia. *Mod. Pathol.* 23, 1251–1260.
- Hernandez, M.R., 2000. The optic nerve head in glaucoma: role of astrocytes in tissue remodelling. *Prog. Retin. Eye Res.* 19, 297–321.
- Jonas, J.B., Jonas, S.B., Jonas, R.A., Holbach, L., Dai, Y., Sun, X., Panda-Jonas, S., 2012. Parapapillary atrophy: histological gamma zone and delta zone. *Plos One* 7 (10), e47237.
- Jonas, J.B., Holbach, L., Panda-Jonas, S., 2014. Peripapillary ring: histology and correlations. *Acta Ophthalmol.* 92, e273–e279.
- Kang, M.H., Yu, D.Y., 2015. Distribution pattern of axonal cytoskeleton proteins in the human optic nerve head. *Neural Regen. Res.* 10, 1198–1200.
- Karimi, A., Rahmati, S.M., Grytz, R.G., Girkin, C.A., Downs, J.C., 2021. Modeling the biomechanics of the lamina cribrosa microstructure in the human eye. *Acta Biomater.* 134, 357–378.
- Lopez, N.N., Clark, A.F., Tovar-Vidales, T., 2020. Isolation and characterization of human optic nerve head astrocytes and lamina cribrosa cells. *Exp. Eye Res.* 197, 108103.
- Marshall, G.E., 1995. Human scleral elastic system: an immunoelectron microscopic study. *Br. J. Ophthalmol.* 79, 57–64.
- May, C.A., 2008. Comparative anatomy of the optic nerve head and inner retina in non-primate animal models used for glaucoma research. *Open Ophthalmol. J.* 2, 94–101.
- Midgett, D.E., Pease, M.E., Jefferys, J.L., Patel, M., Franck, C., Quigley, H.A., Nguyen, T.D., 2017. The pressure-induced deformation response of the human lamina cribrosa: analysis of regional variations. *Acta Biomater.* 53, 123–139.
- Motohashi, O., Suzuki, M., Shida, N., Umezawa, K., Ohtoh, T., Sakurai, Y., Yoshimoto, T., 1995. Subarachnoid haemorrhage-induced proliferation of leptomeningeal cells and deposition of extracellular matrices in the arachnoid granulations and subarachnoid space. *Acta Neurochir.* 136, 88–91.
- Quigley, H.A., Addicks, E.M., 1981. Regional differences in the structure of the lamina cribrosa and their relation to glaucomatous optic nerve damage. *Arch. Ophthalmol.* 99 (1), 137–143.
- Quigley, H.A., Dorman-Pease, M.E., Brown, A.E., 1991. Quantitative study of collagen and elastin of the optic nerve head and sclera in human and experimental monkey glaucoma. *Curr. Eye Res.* 10, 877–888.
- Radius, R.L., Gonzales, M., 1981. Anatomy of the lamina cribrosa in human eyes. *Arch. Ophthalmol.* 99, 2159–2162.
- Roberts, M.D., Liang, Y., Sigal, I.A., Grimm, J., Reynaud, J., Bellezza, A., Burgoyne, C.F., 2010. Correlation between local stress and strain and lamina cribrosa connective tissue volume fraction in normal monkey eyes. *Invest. Ophthalmol. Vis. Sci.* 51, 295–307.
- Shin, A., Yoo, L., Park, J., Demer, J.L., 2017. Finite element biomechanics of optic nerve sheath traction in adduction. *J. Biomech. Eng.* 139. <https://doi.org/10.1115/1.4037562>
- Thale, A., Tillmann, B., Rochels, R., 1996. SEM studies of the collagen architecture of the human lamina cribrosa: normal and pathological findings. *Ophthalmologica* 210 (3), 142–147. <https://doi.org/10.1159/000310694>
- Triviño, A., Ramírez, J.M., Salazar, J.J., Ramírez, A., García-Sánchez, J., 1996. Immunohistochemical study of human optic nerve head astroglia. *Vis. Res.* 36, 2015–2028.
- Voorhees, A.P., Jan, N.J., Austin, M.E., Flanagan, J.G., Sivak, J.M., Bilonick, R.A., Sigal, L.A., 2017. Lamina cribrosa pore shape and size as predictors of neural tissue mechanical insult. *IOVS* 58, 5336–5346.
- Wang, B., Tran, H., Smith, M.A., Kostanyan, T., Schmitt, S.E., Bilonick, R.A., Jan, N.J., Kagemann, L., Tyler-Kabara, E.C., Ishikawa, H., Schuman, J.S., Sigal, L.A., Wollstein, G., 2017. In-vivo effects of intraocular and intracranial pressures on the lamina cribrosa macrostructure. *PLoS One* 12 (11), e0188302.
- Wang, B., Hua, Y., Brazile, B.L., Yang, B., Sigal, L.A., 2020. Collagen fiber interweaving is central to sclera stiffness. *Acta Biomater.* 113, 429–437.
- Wang, X., Rumpel, H., Hoe-Lim, W.E., Baskaran, M., Perera, S., Mongpiur, M.E., Aung, T., Milea, D., Girard, M.J.A., 2016. Finite element analysis predicts large optic nerve head strains during horizontal eye movements. *IOVS* 57, 2452–2462.
- Wang, X., Fisher, L.K., Milea, D., Jonas, J.B., Girard, M.J.A., 2017. Predictions of optic nerve traction forces and peripapillary tissue stress following horizontal eye movements. *IOVS* 58, 2044–2053.
- Wang, X., Guan-Teoh, C.K., Chan, A.S.Y., Thangarajoo, S., Jonas, J.B., Girard, M.J.A., 2018. Biomechanical properties of Bruch's membrane-choroid complex and their influence on optic nerve head biomechanics. *IOVS* 59, 2808–2817.
- Wang, Y.X., Panda-Jonas, S., Jonas, J.B., 2021. Optic nerve head anatomy in myopia and glaucoma, including parapapillary zones alpha, beta, gamma and delta: histology and clinical features. *Prog. Retin. Eye Res.* 83, 100933.
- Zimmer, D.B., Cornwall, E.H., Landar, A., Song, W., 1995. The S100 protein family: history, function, and expression. *Brain Res. Bull.* 37, 417–429.